1D TiO$_2$/0D CdS
Packed structure

Showcasing the study on photoresponses of a uniquely assembled 1D oxide−0D chalcogenide by Prof. Vaidyanathan (Ravi) Subramanian at the SOLAR (Synthesis and Optimization of materials for Light Activated Reactions) laboratory, Department of Chemical and Materials Engineering, University of Nevada, Reno.

Title: A one-pot strategy for coupling chalcogenide nanocrystals with 1D oxides for solar-driven processes

The application of a simple dip coating approach involving an appropriately tailored precursor and a non-planar oxide substrate to achieve a dense coating is demonstrated. The nucleation, growth, and dispersion of chalcogenide nanocrystals can be achieved on the surface of oxides such as 1D TiO$_2$ nanotubes. The assembly demonstrates a stable response to stimulation by light and can be used as an electrode in photoelectrochemical cells.
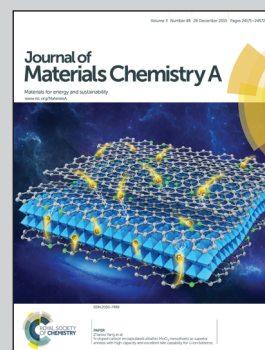
ROYAL SOCIETY
OF CHEMISTRY

www.rsc.org/MaterialsA

A one-pot strategy for coupling chalcogenide nanocrystals with 1D oxides for solar-driven processes†

Pawan Pathak, Satyajit Gupta, Aline C. S. Resende and Vaidyanathan (Ravi) Subramanian*

This work presents a simple approach to the synthesis of CdS coatings on TiO_2 nanotubes (T_NTs) and to form a heterostructured composite. A non-pressure based, single precursor one-pot approach performed at a temperature of 160 °C is used to assemble CdS on the TiO_2 surface. Surface characterization using microscopy, X-ray diffraction, and elemental analysis indicates the formation of dense hexagonal $\langle 002 \rangle$ CdS nanocrystals along the nanotube walls and inter-tubular spacing. Optical measurements indicate that the CdS absorbs in the visible region and demonstrates a red shift with increased loading: up to 12 nm red shift is noted when the precursor concentration is increased from 0.1–3 mM. The 0D CdS/1D T_NT was also tested as an anode in a photoelectrochemical cell. The electrode produced the highest reported photocurrent of 9.3 mA cm^{-2} under UV-visible illumination when compared with similar systems. The method may be used in assembling efficient photoanodes for multifunctional solar-driven processes.

Introduction

Hetero-structured optoelectronic materials (HOMs) are complex structures that consist of a unique combination of a 0D or 1D high surface area substrate (*e.g.* oxide) and a visible light harvester (*e.g.* chalcogenide).[1–4] In such HOMs, the intimate coupling of low bandgap chalcogenide nanocrystals with a wide bandgap oxide surface to facilitate: (i) broad band light absorbance, (ii) facile charge separation/transportation, and (iii) boost the photoanode efficiency is a challenging task. The approaches to assemble such HOMs, that are known today, are either complex (involving multiple steps), require reagents that may be cumbersome to eliminate and risk reducing the HOM photoactivity (such as surfactants),[5] or have building components[6] that can prevent the formation of an intimate electronic contact between the large and small bandgap oxide leading to suboptimal performance of the HOM. Simplifying the integration of oxide–chalcogenide to aid processability with minimal extraneous additives that are not participating in light–matter interactions will be transformational to assemble these materials for various applications. This work presents a simple approach to assemble a representative HOM consisting of a 1D oxide and a 0D chalcogenide nanocrystal.

Standalone chalcogenide synthesis can be achieved using a variety of approaches. For example, the reverse micelle method[7] requires the use of surfactant stabilized micro-emulsions which need to be removed after the synthesis of the chalcogenide. Organic functional group (such as bi-functional linker-'mercaptans') assisted synthesis can aid with size control to improve the optical response, but can interfere with charge transport.[8] Alternately, chalcogenide deposits may also be prepared directly on high surface area oxide films for photoelectrochemical (PEC), photovoltaic (PV), and photocatalytic (PC) applications. The popular 'successive ionic layer adsorption and reaction' (SILAR)[9–11] approach requires several cycles of the layer-by-layer assembly approach to grow cadmium sulfide (CdS) with a high absorbance coefficient. An electrochemical approach[12] requires the application of an external electric field and can limit the extent of deposit formation on a highly intricate surface. Finally, solvothermal approaches can assist with uniform *in situ* nucleation, growth, and coating of chalcogenides, but require a high pressure and time to achieve it.[13] In a recent study, an interesting self-assembly approach to deposit CdS on TiO_2 with a small tube mouth has been reported.[14]

This work presents a facile atmospheric pressure-based 'hot solution dip-casting' strategy (Experimental section in the ESI†) to facilitate *in situ* coupling of the CdS nanocrystals with the titania (TiO_2) surface. The method demonstrated a uniform coverage of the CdS nanocrystals over the TiO_2 nanotube (T_NT) surface with the highest photocurrent compared to any other wet chemical approach reported to date using T_NT and

Chemical and Materials Engineering Department, University of Nevada, Reno, 1664 N. Virginia Street, Reno, Nevada 89557, USA. E-mail: ravisv@unr.edu; Fax: +1-775-327-5059; Tel: +1-775-784-4686

This journal is © The Royal Society of Chemistry 2015

J. Mater. Chem. A, 2015, **3**, 24297–24302 | 24297

chalcogenide-based systems. Earlier, we have shown various approaches to integrate chalcogenides with oxide substrates of the 0D and 1D configuration.[15,16] This approach to integrate a chalcogenide with a 1D oxide substrate is a simple wet chemical technique for this class of chalcogenide-based composites, especially considering the magnitude of the current that we are able to achieve. The unique aspects of this work include (i) using a one-pot approach with cadmium (Cd) and sulfur (S) from the same precursor, in order to nucleate, deposit, and grow CdS on 1D oxide with no extraneous additives, (ii) demonstrating the same or higher magnitudes of photocurrents compared to the values reported with other complex approaches, and (iii) improved stability of the photoresponse compared to composites formed using other techniques. This work also presents comparative results with T_NT/CdS prepared by the SILAR approach.[17,18] The SILAR approach was used as a benchmark comparison since this approach has been reported extensively and considered one of the low cost, reliable, and easily scalable methods for CdX (X = S, Se, Te) formation on both 0D and 1D-oxide facades.

Experimental

Materials

Sodium diethyldithiocarbamate [$(C_2H_5)_2NCS_2Na$)], ammonium fluoride (NH_4F), cadmium sulfate ($CdSO_4$) (from Sigma Aldrich), oleylamine (Across Organics), titanium foil (purity: 99.7%, 0.2 mm thick, Strem Chemicals Inc), dichloromethane, ethylene glycol and ethanol (from local suppliers), and deionized (D.I.) water (Millipore® lab water purification system) were used as received without further purification.

Synthesis procedure

Titanium foil was used to prepare the titanium nanotubes (T_NTs) as described in our earlier studies.[19] Briefly, the titanium substrate was polished and ultrasonicated with DI water, isopropanol, and acetone separately for 5 minutes each. Fluorinated solution (0.5% w/w) of ethylene glycol and DI water (10% w/w) was used as an electrolyte. Anodization was done in the two electrode system with platinum as the reference electrode using 40 V DC power supply for 2–16 h. Anodized samples were annealed at 450 °C for 2 h in air.

The cadmium dithioarbamate Cd[$(C_2H_5)_2NCS_2]_2$ precursor was synthesized by mixing 0.1 M aqueous solution of $CdSO_4$ into 0.2 M aqueous solution of $(C_2H_5)_2NCS_2Na$ for 3 h.[20] The resulting solution immediately started precipitating. The white precipitate was then[2] washed thoroughly with DI water and dried in an oven for 6 hours at 50 °C.

At first 30 mL of oleylamine was heated at a temperature of 160 °C, and then T_NTs prepared at various anodization times were dipped in the oleylamine solution. After 5 min, the cadmium dithiocarbamate precursor (of various concentration values, 0.1 mM, 0.5 mM, 1 mM, 2 mM and 3 mM) was added into the solution and kept at 160 °C for 40 min. To remove the organic ligand the sample was dipped into ethanol and dichloromethane separately for 8 h. To get better crystallinity,

the sample was annealed at 350 °C for 3 h in a nitrogen atmosphere. A schematic of the method is shown in the ESI† section and the photographs of the T_NT sample with various concentrations of the Cd precursor are also provided.

Characterization

The UV-visible absorbance studies were performed using a Shimadzu UV-2501PC spectrophotometer in the range of 300 nm–900 nm, in absorbance mode. Imaging of the samples was carried out using a Hitachi FESEM scanning electron microscopy (SEM) machine equipped with an oxford EDS analyzer. The cross-sectional morphology of the electrodes was observed by scratching the samples with a sharp object. A JEOL® 2100F high resolution transmission electron microscope (HR-TEM) was used to examine the size of CdS deposits on the T_NT surface. A Philips XRG 3100 X-ray diffractometer, operating at 35 kV, was used to obtain the X-ray diffraction pattern and identify the phase of the material after each annealing step, in the film form.

The photoelectrochemical studies were carried out in a three-electrode system, using a quartz cell with Pt mesh as a counter electrode and a leak free Ag/AgCl (in 3 M KCl) as the reference electrode. 0.1 M Na_2S in water was used as the electrolyte. J/t and J/V characteristics were collected using an Autolab PGSTAT 30 electrochemical analyzer. The same instrument was used for performing electrochemical impedance measurements. The working electrode was irradiated with a 500 W Newport xenon lamp equipped with 0.5 M $CuSO_4$ solution as a far UV cut-off filter; this also attenuates the light intensity to ~90 mW cm^{-2}. All the impedance measurements were carried out using the same electrochemical set-up described above, with 0.1 N KCl as an electrolyte. Photoluminescence (PL) spectra of the samples were measured using a Fluoromax-3 Horiba Fluorimeter.

Results and discussion

The scanning electron microscopy (SEM) image shown in Fig. 1A indicates cylindrical and well developed TiO_2 nanotube arrays (T_NTs) following anodization of titanium (Ti) foil. The inset of Fig. 1A shows the cross-sectional view of the nanotube surface. The nanotubes are of ~100 nm in diameter, with distinct interstitial spaces between the adjacent tubes. Post one-pot treatment, uniform coverage (coating thickness of ~30 nm) can be observed all over the T_NTs as shown in Fig. 1B. The inset of Fig. 1B shows the cross-sectional view of the nanotube surface with the deposits. Additional cross-sectional SEM images of the bare nanotubes (Fig. S1(A), ESI†) and with the deposits (Fig. S1(B), ESI†) show that the deposits are present along the mouth and the T_NT walls while the nanotube mouth mostly remains open. This form of deposition is desirable as it can minimize clogging of the T_NT mouth and improve photocurrent generation by maximizing electrolyte transport. It is noteworthy to mention that the approaches that use preformed nanoparticles with nanotubes risk significant clogging of the pore mouth. In this approach, the nanocrystals are

24298 | *J. Mater. Chem. A*, 2015, **3**, 24297–24302

This journal is © The Royal Society of Chemistry 2015
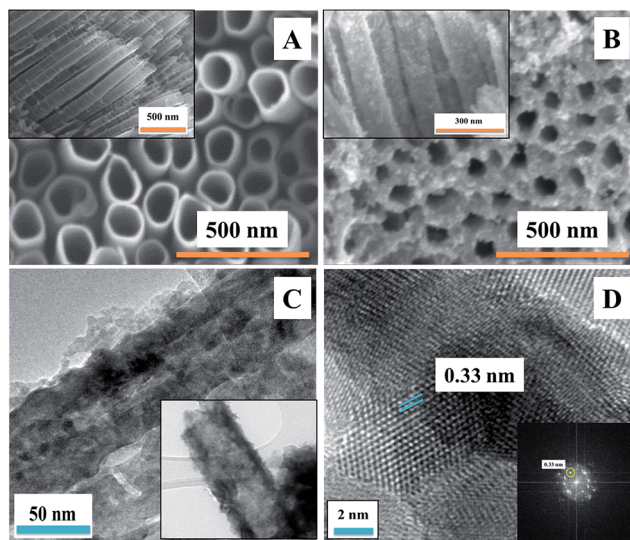
Fig. 1   (A) SEM image of bare T_NTs; inset: cross sectional view of the smooth T_NT surface, (B) SEM image of bare T_NTs with optimized CdS (prepared using 2 mM precursor); inset: cross sectional view of the T_NT/CdS surface, (C) TEM image of bare T_NTs with CdS deposited by the one-pot method on the T_NT surface, (D) TEM image of the as-deposited CdS on the T_NT surface indicating an average particle size of 10 ± 5 nm; (inset: FFT diffraction pattern).

formed on the oxide surface after diffusion of the precursor into the Ti sites followed by their nucleation and growth. The T_NTs with varying amounts of deposits prepared using precursors of different concentrations are shown in Fig. S2(A)–(C), ESI.†

Transmission electron microscopy (TEM) without and with high resolution imaging (HR-TEM) was performed on the HOM to determine the surface and composition of the materials. Fig. 1C shows the cross-section of a representative sample with the deposits. TEM images of the deposits at various magnifications are shown in Fig. S3(A) and (B), ESI.† The images confirm the observations made by SEM that the deposits formed are dense and continuous. They are distinctly evident along the walls attaching credence to the earlier hypothesis that the crystals are formed after the precursor diffuses along the interstitial spaces and nucleate on the surface. Fig. 1D shows the HR-TEM image of the deposits. The deposits are of 10 ± 5 nm in diameter. Further, they demonstrate crystallinity as evident from the fringe pattern in the HR-TEM image as well as the high resolution Fast Fourier Transformation (FFT) pattern in the inset of Fig. 1D. These fringes can be indexed to the ⟨002⟩ plane enabling the identification of the deposits as CdS nanocrystals. The TEM image with additional 'd-spacing' values is indicated in Fig. S4(A), ESI† and the FFT image is shown in Fig. S4(B), ESI.† These images indicate the polycrystallinity of CdS and confirm the deposits as the ⟨002⟩ plane of hexagonal CdS.

Additional comprehensive material characterization was achieved by performing color resolution mapping analysis of the elements. This specialized technique can provide insights into the distribution of the elemental cadmium (Cd), sulfur (S), and titanium (Ti). The decoupled colour mapping of the

building block units in the HOM – Cd, S, and Ti – is shown in Fig. 2(A1) to (A3). These images also indicate that the one-pot approach leads to homogeneous distribution of CdS. The color mapping analysis is a convincing cross-verification of the microscopy analysis in which the CdS is found distributed along the cross-sectional length of nanotubes. Further, the energy dispersive X-ray spectroscopy (EDAX) analysis shown in Fig. 2(A4) indicates that the deposits are Cd-rich (Fig. 2(A4) inset). This form of uniform and robust distribution is a prerequisite to any application. For example, if the photoelectrochemical process is the primary objective, an excellent electronic contact between the two semiconductors is critical and will determine the magnitude of the photocurrent generated by the HOM.

The surface and optical properties of the HOM architecture were analysed using X-ray diffraction (XRD) and UV-visible spectroscopy. The XRD patterns of the nanotube and nanotube with the deposits are shown in Fig. 3(A(a) and (b)), respectively. The indexing of the peaks to file # 21-1272 and file # 41-1049 of the JCPDS database confirms that the nanotubes comprise of anatase TiO_2 and the deposits are hexagonal CdS. The absorbance spectra of T_NTs with various 'Cd' precursor concentrations are shown in Fig. 3B. The evidence of an onset at ~515 nm is consistent with the location where the CdS nanocrystal absorbance should appear. The gradual red-shift in the absorbance value (516 nm → 528 nm) with increased precursor concentration is indicative of the growth and densification of the CdS nanocrystals on the T_NT. Thus the SEM, HR-TEM, EDAX, color mapping, and absorbance results complement one another and confirm that the one-pot approach is an effective strategy for the deposition and growth of hexagonal type 0D CdS on the 1D TiO_2 nanotubes.

The photoelectrochemical responses of the HOMs were examined in a two and three electrode (with reference Ag/AgCl)
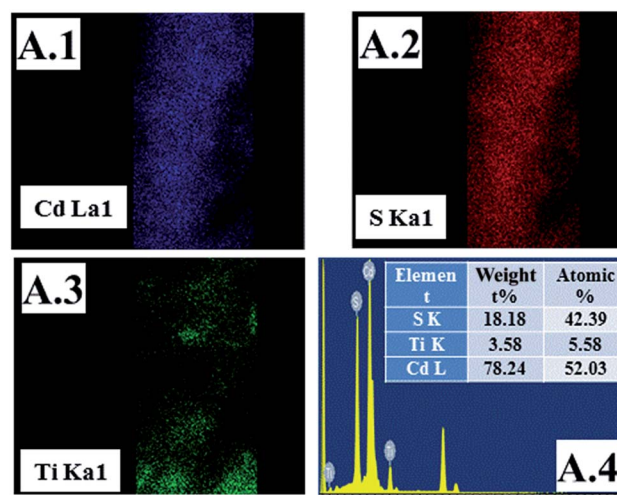
Fig. 2   (A1–A3) Cd, S, and Ti distribution on the T_NT/CdS is evident from the color coding which indicates the spread of the different elements [images are best viewed in color]. (A4) The EDAX analysis of the deposited CdS over the T_NT surface indicates the relative composition of the different elements on the T_NT/CdS heterostructure.
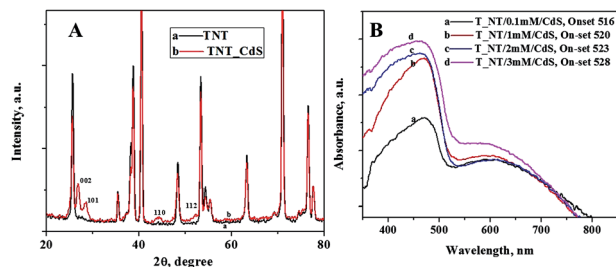
Fig. 3 (A) The XRD pattern of bare T_NTs and CdS deposited T_NTs prepared by the one-pot method. The polycrystalline nature of the film is evident from the signals. (B) The UV-visible absorbance spectrum of T_NTs, deposited with CdS at various precursor concentrations. The presence of CdS shows a visible absorbance ranging between 516 nm and 528 nm.

configuration. Chronoamperometry (J/t) measurements of the films are shown in Fig. S5(A), ESI.† The results indicate that the UV-visible illumination leads to an instantaneous and reproducible response as evident from the several on–off cycles. The presence of CdS, prepared using a low precursor concentration of 0.1 mM, shows a positive increase compared to the CdS-free T_NT. At 6.3 mA cm^{-2}, a maximum in the photocurrent is observed at a CdS loading with 2 mM precursor concentration [an increase of ~30-fold over the bare T_NT]. Any further increase in the CdS loading leads to reduction in the photocurrent.

The current density/voltage (J/V) analysis indicates the photocurrent response of the HOMs at various applied potentials Fig. S5(B), ESI.† All the CdS deposited samples show higher photocurrent compared to the T_NT at any applied potential. Further, a negative shift in the apparent flat band potential (potential where the current becomes zero) with all the CdS deposits is noted, with the highest shift observed for the CdS deposits prepared using the 2 mM precursor. The negative shift is indicative of the charge generation, accumulation, and transport upon photo-illumination in the HOM. It may be noted that the samples made using the 2 mM precursors demonstrate nearly the same photocurrent as those prepared using the 3 mM after few hundreds of seconds. Therefore, we studied the long-term stability of both samples. After ~100 minutes it is observed that the 2 mM sample is more stable than the 3 mM sample as indicated in Fig. S5(C).† The scheme in the Fig. S5(C) ESI† inset shows the mechanism of charge generation, separation, and transport in the HOM.

To evaluate the novelty and determine the limits of the HOM synthesis strategy, we performed a systematic and thorough literature survey of the 1D TiO$_2$-0D QD systems and compared the photoactivity reported therein with our results. Fig. S(6), ESI,† shows the table listing the leading photocurrent results using 1D TiO$_2$ with chalcogenides to date. There are few systems that show the photocurrent values similar to the magnitude reported here. On close examination of the approach used to synthesize the composites in the cited work, it may be noted that the approach presented here stands out along the following aspects: (i) this work has demonstrated a one-pot approach to form CdS nanocrystals at the 1D TiO$_2$ surface using a single-precursor as a simultaneous 'Cd' and 'S' source under atmospheric conditions, (ii) a point to be considered is the processing time. With the popular SILAR approach, depending upon the number of cycles employed, it can add up quickly and become a time consuming step while with the present process the removal of the organic ligand can take a long time (~18 h). However, the time required for coupling is the lowest compared to the procedure used in the synthesis of the other composites. For example, it is 1/6th of the time required when compared to the sample that is reported to show a current-density of 6 mA cm^{-2}, and (iii) the CdS deposition appeared to be uniform and provided an intimate contact, which probably is the reason why our HOM demonstrates high photocurrent. It will be inferred from studies presented below that a better utilization of the CdS is the basis for this observation.

Further, electrochemical measurements were conducted on T_NT/CdS to gather quantitative information on its performance. Fig. 4A shows the PL spectra of the T_NT/CdS prepared using the SILAR and the one-pot method (λ_{ex} = 340 nm). The two peaks around 520 and 560 nm are the resultant of the intermediate quenching between the CdS nanoparticle and T_NT.[21,22] These peaks are caused by the radiative recombination of the electron–hole pairs between the interface of the CdS and T_NT. From the figure, the T_NT/CdS sample prepared using the one-pot approach exhibits a weaker peak intensity than the sample prepared using the SILAR approach. A lower quenching is attributed to better charge separation.[21] Further, the electrochemical impedance spectra (EIS) were acquired to compare the performance of the CdS deposited on T_NTs by the SILAR and the one-pot approach. Nyquist and Bode plots offer scientific reasoning through impedance measurements on the nature of electrical contact that exists in composite materials.[23] Specifically, the charge transfer resistance is proportional to the diameter of the arc of the Nyquist plot at constant bias voltage.
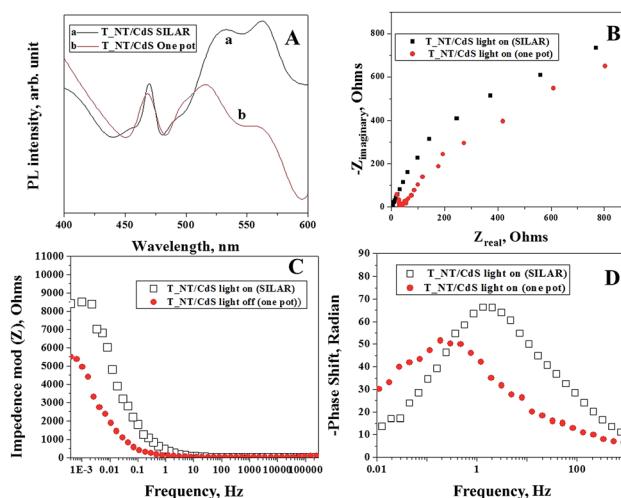
Fig. 4 Collage of photoluminescence spectra and EIS of CdS deposits on T_NTs prepared with the SILAR and one-pot method. The figures present (A) photoluminescence spectra, (B) Nyquist plot, (C) Bode plots representing the variation in the magnitudes of impedance with frequency, and (D) phase angle with frequency.

The complex impedance plane or Nyquist plot (Fig. 4B) suggests that the charge transfer resistance is higher for the CdS deposited sample with the SILAR approach than that prepared using the one-pot method. Fig. 4C and D compare the results of the Bode impedance plot for the SILAR and the one-pot approach. Here as well, CdS deposited by the SILAR approach shows a higher impedance than the deposits prepared by the one-pot approach. Further, from the Bode phase plot, quantitative information such as the average life time of the electron can be calculated using the following equation:[23] $\tau = 1/2\pi f_p$ where f_p is the characteristic frequency of the samples, related to electrochemical reaction at TiO_2/CdS and the electrolyte interface. The SILAR coupled sample has the electron life time (τ) of 94 ms and that of one-pot is 516 ms which indicates that the electron transfer process to the TiO_2 channel and the flow of the electron from the conduction band of CdS to TiO_2 is more effective in the one-pot synthesized HOM compared with the SILAR method. Thus, PL, Nyquist, and Bode analyses indicate that the one-pot approach enables establishing a strong contact between T_NTs and CdS lowering the recombination of the photo-induced electron–hole pairs in the HOM.

A logical question then arises: *What will be the change in the photocurrent with respect to change in the anodization time?* To answer this question, anodization was performed for a duration of 2–16 h. As indicated in Fig. S5(D), ESI,† a T_NT sample anodized for 12 h demonstrated the best photocurrent when compared to T_NT anodized for 2 h, 8 h, 12 h, and 16 h. These results are attributable to greater CdS deposit formation over T_NTs of increased length. Any further increase in the anodization time beyond 12 h makes T_NTs more unstable due to the delamination of some of the tubes from its base. Due to this CdS deposition is flaky and the photocurrent is decreased. The J/t and J/V responses of the 12 h anodized samples are shown in

Fig. 5A and B, since this condition is considered optimal for the system. To the best of our knowledge, a current of 9.3 mA cm^{-2}, demonstrated with the 12 h anodized sample here, is a significant improvement when specifically compared with systems involving 3-electrodes, Na_2S redox couple, and CdS as the sensitizer using accepted protocols published elsewhere. (see Fig. S(6), ESI†). A sub-set of the compared references uses the T_NT/CdS, Na_2S electrolyte, and Ag/AgCl reference electrode. On another related note, it is known that CdS is prone to corrosion and hence its stability is of critical importance to any performance evaluation. Therefore, chronoamperometry measurements were performed to evaluate the HOM stability. The photocurrent magnitude was noted to reduce under continuous illumination by only 40% over a period of 1 h. The results of a comparison with SILAR approach are given in Fig. 5C. A ~50% decrease in the photocurrent was observed for SILAR samples in spite of the photocurrent starting at a lower value. While this result is a promising step in the right direction, it also indicates room for improvement in stabilizing the T_NT/CdS response and highlights the potential of the one-pot approach to help realize competitively stable HOMs.

Conclusions

A one-pot approach to assemble a T_NT/CdS nanostructured composite is presented. SEM, (HR) TEM, XRD, and color mapping provide a detailed insight into the assembly and structure of the nanocomposite. At 9.3 mA cm^{-2} the photocurrent value is the best achieved using this one-pot methodology. Using PL and EIS studies, the scientific reasoning for the improvement is determined as the existence of an excellent electronic contact between the T_NT and CdS. The results should lay the foundation for designing and developing other HOMs involving several combinations of nanocrystals, such as CdX (X = Se, Te). Further, multiple nanocrystals can be coupled to realize 'rainbow' absorbance as indicated in the schematic of Fig. 5D. The presented approach could be adapted to realizing such an assembly in an easier, effective, and cost-competitive manner. Obviously, key parameters such as tube dimensions, spacing, matching of appropriate energetics (such as conduction band levels of the nanocrystals) have to be examined for optimal photoanode performance. This approach is expected to impact the materials synthesis strategies used in composite electrode driven applications in the area of photoelectrochemistry, PV, solar-fuels and other allied topics of energy storage and sensing.

Acknowledgements

Notes and references

1 B. Mukherjee, A. Peterson and V. Subramanian, *Chem. Commun.*, 2012, **48**, 2415–2417.
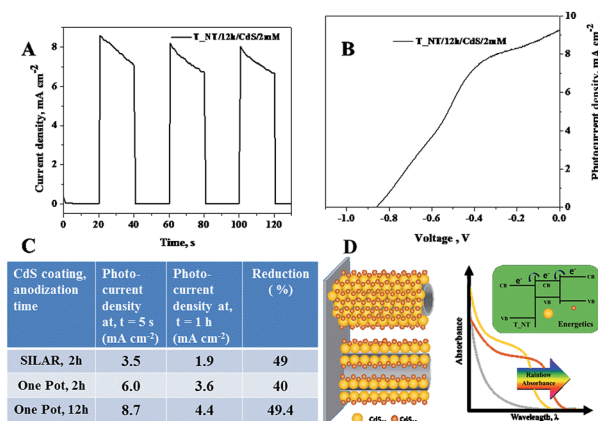
Fig. 5 (A) J/t and (B) J/V plot of T_NTs, deposited with CdS over T_NTs anodized for 12 h, measured in a three-electrode system, using a quartz cell with Pt mesh as a counter electrode and a leak free Ag/AgCl (in 3 M KCl) as the reference electrode. 0.1 M Na_2S in water was used as the electrolyte. The working electrode was illuminated with a 500 W Newport xenon arc lamp equipped with 0.5 M $CuSO_4$ solution as a far UV cut-off filter, (C) the table shows the photocurrent values of the T_NT/CdS illuminated for 1 h. Note the CdS deposit is prepared between 2 and 12 h (see text for details), and (D) hypothesis for the fabrication of a photoanode with a "rainbow" architecture.

CdS coating, anodization time	Photo-current density at, t = 5 s (mA cm^{-2})	Photo-current density at, t = 1 h (mA cm^{-2})	Reduction (%)
SILAR, 2h	3.5	1.9	49
One Pot, 2h	6.0	3.6	40
One Pot, 12h	8.7	4.4	49.4

2 A. A. Lutich, C. Mauser, E. D. Como, J. Huang, A. Vaneski, D. V. Talapin, A. L. Rogach and J. Feldmann, *Nano Lett.*, 2010, **10**, 4646–4650.

3 S. Liu, Z. Tang, Y. Sun, J. C. Colmenares and Y. Xu, *Chem. Soc. Rev.*, 2015, **44**, 5053–5075.

4 B. Weng, S. Liu, Z. Tang and Y. Xu, *RSC Adv.*, 2014, **4**, 12685–12700.

5 J. Li, M. W. G. Hoffmann, H. Shen, C. Fabrega, D. J. Prades, T. Andreu, F. Hernandez-Ramirez and S. Mathur, *J. Mater. Chem.*, 2012, **22**, 20472–20476.

6 I. Robel, V. Subramanian, M. K. Kuno and P. V. Kamat, *J. Am. Chem. Soc.*, 2006, **128**, 2385–2393.

7 H. Zhang, L. P. Wang, H. M. Xiong, L. H. Hu, B. Yang and W. Li, *Adv. Mater.*, 2003, **15**, 1712–1715.

8 A. Kongkanand, K. Tvrdy, K. Takechi, M. Kuno and P. V. Kamat, *J. Am. Chem. Soc.*, 2008, **130**, 4007–4015.

9 D. R. Baker and P. V. Kamat, *Adv. Funct. Mater.*, 2009, **19**, 805–811.

10 M. A. Becker, J. G. Radich, B. A. Bunker and P. V. Kamat, *J. Phys. Chem. Lett.*, 2014, **5**, 1575–1582.

11 P. Pathak, S. Gupta, K. Grosulak, H. Imahori and V. Subramanian, *J. Phys. Chem. C*, 2015, **119**, 7543–7553.

12 P. K. Santra, P. V. Nair, K. G. Thomas and P. V. Kamat, *J. Phys. Chem. Lett.*, 2013, **4**, 722–729.

13 B. Mukherjee, Y. R. Smith and V. Subramanian, *J. Phys. Chem. C*, 2012, **116**, 15175–15184.

14 F. Xiao, J. Miao, H. Wang and B. Liu, *J. Mater. Chem. A*, 2013, **1**, 12229–12238.

15 B. Mukherjee, S. Gupta, A. Manivannan, H. Imahori and V. Subramanian, *Chem. –Eur. J.*, 2014, **20**, 10456–10465.

16 Y. R. Smith and V. Subramanian, *J. Phys. Chem. C*, 2011, **115**, 8376–8385.

17 R. Zhou, H. Niu, Q. Zhang, E. Uchaker, Z. Guo, L. Wan, S. Miao, J. Xu and G. Cao, *J. Mater. Chem. A*, 2015, **3**, 12539–12549.

18 Q. Kang, S. Liu, L. Yang, Q. Cai and C. A. Grimes, *ACS Appl. Mater. Interfaces*, 2011, **3**, 746–749.

19 Y. Sohn, Y. Smith, M. Misra and V. Subramanian, *Appl. Catal., B*, 2008, **84**, 372–378.

20 S. Shen, Y. Zhang, L. Peng, B. Xu, Y. Du, M. Deng, H. Xu and Q. Wang, *CrystEngComm*, 2011, **13**, 4572–4579.

21 K. Das and S. K. De, *J. Phys. Chem. C*, 2009, **113**, 3494–3501.

22 J. J. Liqiang, Q. Yichun, W. Baiqi, L. Shudana, J. Baojiang, Y. Libin, F. Wei, F. Honggang and S. Jiazhong, *Sol. Energy Mater. Sol. Cells*, 2006, **90**, 1773–1787.

23 A. J. Bard and L. R. Faulkner, *Electrochemical Methods*, John Wiley and Sons, 2nd edn, New Jersey, 1980.

24302 | *J. Mater. Chem. A*, 2015, **3**, 24297–24302

This journal is © The Royal Society of Chemistry 2015